Available online at www.sciencedirect.com
SCIENCE DIRECT
ELSEVIER
International Journal of Mass Spectrometry 254 (2006) 168–182
International Journal of Mass Spectrometry
www.elsevier.com/locate/ijms

Why is hafnium so unreactive? Experimental and theoretical studies of the reaction of Hf^+ with methane

Laura G. Parke, Christopher S. Hinton, P.B. Armentrout *

Department of Chemistry, University of Utah, Salt Lake City, UT 84112-0850, USA

Received 19 April 2006; received in revised form 27 May 2006; accepted 29 May 2006
Available online 7 July 2006

Abstract

The reaction of atomic hafnium cations with CH_4 and CD_4 is studied using a guided ion beam tandem mass spectrometer. In contrast to most third-row transition metal ions, the dehydrogenation reaction to form $HfCH_2^+ + H_2$ is endothermic. At higher energies, other products, $HfCH^+$, $HfCH_3^+$, and HfH^+, the latter being the predominant species, are observed. Implicit in the behavior of the cross sections for HfH^+, $HfCH_2^+$, and $HfCH_3^+$ is a $H{-}Hf^+{-}CH_3$ intermediate. Modeling of the endothermic cross sections provides for 0 K bond dissociation energies (in eV) of $D_0(Hf^+{-}CH) = 5.10 \pm 0.15$, $D_0(Hf^+{-}CH_2) = 4.37 \pm 0.07$, $D_0(Hf^+{-}CH_3) = 2.12 \pm 0.26$, and $D_0(Hf^+{-}H) = 1.97 \pm 0.11$. These experimental bond energies are in good agreement with density functional calculations at the B3LYP/HW+/6–311 ++ G(3*df*,3*p*) level of theory. Theoretical calculations reveal the mechanism of the reaction and illustrate the geometric and electronic structures of the individual products and intermediates. Unlike its first and second-row congeners, which have quartet ground states and must change spin to dehydrogenate methane, Hf^+ retains its ground state doublet configuration throughout the dehydrogenation reaction, demonstrating that spin-restrictions are not responsible for the relatively low reactivity of Hf^+. Instead, this can be attributed to the unfavorable doubly occupied 6*s* orbital in the ^2D ground state of Hf^+.

Keywords: Bond dissociation energies; C—H bond activation; Guided ion beam mass spectrometry; Hafnium; Methane

1. Introduction

In understanding catalysis, it is useful to consider not only which systems are reactive but also which systems are not. If the underlying reasons for the differences can be quantitatively assessed, the results can lend considerable insight into the electronic and geometric details that enhance (or suppress) reactivity. A case in point is the reactions of atomic metal ions with methane. Activation of methane is of considerable interest as identification of a convenient catalyst for selective oxidation to methanol would be technologically important by allowing better use of natural gas [1,2]. Further, the C–C coupling reactions intrinsic to Fischer-Tropsch chemistry have been observed to occur for the two early third-row transition metal ions, Ta^+ and W^+, in the gas phase [3,4]. Oddly, Hf^+, the other early third-row transition metal ion, fails to react with methane at thermal energies, even though its second-row analogue, Zr^+, is probably the most reactive second-row transition metal ion [5,6], and Ti^+, its first-row congener, is certainly one of the more reactive first-row transition metal ions [7,8].

The ground state of Hf^+ is ^2D with a $6s^25d^1$ electronic configuration, whereas the ground states of Ta^+ (^5F, $6s^15d^3$), W^+ (^6D, $6s^15d^4$), Zr^+ (^4F, $5s^14d^2$), and Ti^+ (^4F, $4s^13d^2$) all have half-filled valence *s* orbitals. Indeed, hafnium is one of only two transition metal cations to have such an s^2 configuration as its ground state, Lu^+ being the other. For all other transition metal cations, the s^2d^{n-2} configuration has a relatively high energy compared to the s^1d^{n-1} or d^n states. For lutetium and hafnium, the s^2 configuration is low in energy because of the lanthanide contraction, a result of relativistic effects. Because of this closed shell configuration, Lu^+ (^1S, $6s^2$) has long been known to be very unreactive with methane [9]. On the basis of similar observations for the other third-row metal ions, Irikura and Beauchamp suggested that the reactivity of the transition metal cations with methane can be correlated with the accessibility of the s^1d^{n-1} configuration [3,4], such that Hf^+ (^2D) will not be reactive, in good

* Corresponding author. Tel.: +1 801 581 7885; fax: +1 801 581 8433.
E-mail address: armentrout@chem.utah.edu (P.B. Armentrout).

1387-3806/$ – see front matter © 2006 Elsevier B.V. All rights reserved.
doi:10.1016/j.ijms.2006.05.025

correspondence with reactivity rules thoroughly evaluated for the first-row transition metal cations [7,10]. However, the question remains why Hf^+ does not react more efficiently by coupling to its ^4F ($6s^15d^2$) excited state, which lies only 0.56 eV higher in energy [11], especially as spin–orbit coupling effects are large for the third-row metals.

Previous experimental studies concerning the reaction of Hf^+ with methane were performed at thermal energies by Irikura and Beauchamp using a Fourier transform ion cyclotron resonance (FTICR) mass spectrometer [3,4]. They did not observe a reaction for thermal Hf^+, although residual excited states did react. Furthermore, they found that $HfCH_2^+$ is readily reduced back to Hf^+ by dihydrogen, verifying that the dehydrogenation reaction with methane is endothermic. To further explore why Hf^+ is so unreactive, a more quantitative characterization of the thermochemistry and a thorough exploration of the potential energy surface would be desirable. In the present study, we investigate the reactions of Hf^+ with CH_4 and CD_4 over a wide range of kinetic energies such that several $HfCH_x^+$ species are formed. All processes observed are endothermic, thereby allowing the determination of the bond energies of these species and providing mechanistic information about the reactions. Complementing these experimental studies is a thorough theoretical examination of the potential energy surface and all intermediates and products.

2. Experimental and theoretical methods

2.1. General procedures

These experiments were carried out using a guided ion beam tandem mass spectrometer described in detail elsewhere [12,13]. Ions are generated in a source described below, extracted from the source, accelerated and focused into a magnetic sector momentum analyzer for mass analysis. The ^{180}Hf isotope (35.2% natural abundance) is selected, decelerated to a desired kinetic energy and then focused into an octopole ion beam guide. Radio frequency electric fields trap the ions in the radial direction for complete collection of reactant and product ions [14,15]. As the ions travel down the octopole, they pass through a static gas cell that holds the neutral reactant at low pressures (<0.3 m Torr) to ensure single collision reaction conditions. This was confirmed through the examination of the pressure dependence of the cross sections measured.

The unreacted parent and product ions drift to the end of the octopole where they are extracted and focused into a quadrupole mass filter for mass separation. A secondary electron scintillation detector is used to detect ions using standard pulse counting techniques. After accounting for background signals, reaction cross sections are calculated from product ion intensities as compared to reactant ion intensities [16]. Uncertainties in absolute cross sections are estimated to be ±20%.

The octopole is used as a retarding energy analyzer to determine the absolute zero and distribution of the ion kinetic energy by varying the dc bias on the octopole rods relative to the potential of the ion source region [16]. Laboratory (lab) ion energies are converted to energies in the center-of-mass frame (CM) using $E_{CM} = E_{lab} \times m/(m+M)$, where m and M are the neutral and ionic reactant masses, respectively. Reaction cross sections are broadened by the kinetic energy distribution of the reactant ion and the random thermal motion of the reactant molecules in the gas cell (Doppler broadening) [17]. The distributions of ion kinetic energies are independent of energy and are close to Gaussian with a typical fwhm of 0.6–0.9 eV (lab).

2.2. Ion source

Hf^+ ions are generated in a direct-current discharge flow tube (DC/FT) source that uses a hafnium cathode held at a high negative voltage (0.7–1.5 kV) over which a flow of approximately 90% He and 10% Ar passes at an average pressure of 0.3–0.4 Torr [13]. Ar^+ ions created in the discharge are accelerated toward the hafnium cathode creating atomic metal ions. Subsequently, the ions undergo $\sim 10^5$ collisions with He and $\sim 10^4$ collisions with Ar as they travel down the 1-m long flow tube prior to entering the ion beam apparatus. In previous studies, it has been demonstrated that the electronic temperature of atomic metal ions produced in the flow tube source ranges between 300 and 1100 K [18–22]. Thus, even at the maximum likely temperature, 98.9% of the hafnium ions are in the ^2D ground state, and 96.2% in the $^2D_{3/2}$ ground level (99.9 and 99.7%, respectively, at the average temperature of 700 K). The average electronic energy, E_{el}, for Hf^+ at a temperature of 700 ± 400 K is $0.006 + 0.010/-0.006$ eV.

2.3. Data analysis

Data analysis of the kinetic energy dependence of product cross sections is performed to determine the energy threshold for product formation, E_0. The apparent threshold observed under laboratory conditions is shifted from this E_0 because of the Maxwell–Boltzmann velocity distribution of the neutral reactants, as well as the kinetic and internal energy distributions of the reactant ions. These effects cause reactions to take place at energies below E_0. It has been shown in previous theoretical and experimental work that endothermic cross sections can be modeled using Eq. (1) [23–25],

$$\sigma(E) = \frac{\sigma_0 \Sigma g_i (E + E_i + E_{el} - E_0)^n}{E} \quad (1)$$

where σ_0 is an energy-independent scaling parameter, E the relative kinetic (translational) energy of the reactants, E_0 the reaction threshold at 0 K, and n an adjustable parameter that determines the shape of the cross section. The summation is over all possible rovibrational states of the neutral reactant with populations g_i ($\Sigma g_i = 1$) and energies E_i. The vibrational frequencies and rotational constants used in determining E_i are taken from the literature for CH_4 and CD_4 [26]. The electronic energy of the Hf^+ reactant is $0.006 + 0.010/-0.006$ eV, as noted above. The model of Eq. (1) is convoluted over the neutral and ion kinetic energy distributions prior to comparison with the data [16,24,25]. The adjustable parameters are then optimized using a nonlinear least-squares analysis to give the best reproduction of the data. Values reported for E_0, σ_0, and n are the average values obtained for

each parameter over a range of best fits to several independent data sets. The corresponding uncertainties are one standard deviation. Uncertainties in the absolute energy scale (±0.05 eV, lab) and the uncertainty in the electronic energy of Hf^+ are included in the uncertainties reported for E_0.

As discussed below, the reaction channels observed probably compete with one another, which could have an influence on the thresholds of the higher energy channels. Although we have developed a simple statistical approach to model competition [27], this approach is not sufficient for the present system as some channels (including the entrance channel, see below) have tight transition states that will influence the competition. Ideally, a phase space approach in which angular momentum is explicitly considered is needed to accurately model these bimolecular reactions, but again the presence of a barrier in the entrance channel in addition to the transition states for some channels makes such an approach too difficult to obtain accurate results.

2.4. Theoretical calculations

Most quantum chemistry calculations here are computed with the B3LYP hybrid density functional method [28,29] and performed using the Gaussian 03 suite of programs [30]. This level of theory was chosen because it provides reasonable results for reactions of methane with Pt^+ [31], Re^+ [32], W^+ [33], and Ir^+ [34]. The relatively large 6–311 ++ G(3*df*,3*p*) set is used for carbon and hydrogen because of the bridging hydrogens that occur for many of the transition states of interest. This basis set yields bond dissociation energies (BDEs) for the hydrocarbon species in close correspondence (within 0.08 eV) with experimental BDEs: H–CH_3 (4.406 versus 4.480 eV), H_2–CH_2 (4.666 versus 4.713 eV), H–CH (4.332 versus 4.360 eV), C–H (3.532 versus 3.465 eV) and H–H (4.505 versus 4.478 eV) [31]. The relativistic effective core potential (ECP) of Hay-Wadt (HW) [35] is used to describe the 60 core electrons of hafnium and the Los Alamos double-ζ basis set (LANL2DZ) is used to describe the valence electrons. This basis set is optimized for neutral atoms, whereas the charge differentially contracts the 6*s* orbitals compared to the 5*d* orbitals. This is accounted for in an altered valence basis set described by Ohanessian et al. [36], designated as HW +, which is used for most of our calculations.

First- and third-row transition metal methyl cations have been thoroughly investigated by Holthausen et al. [37], and first-row transition metal methylene cations by Holthausen et al. [38]. In the first study, calculations were performed using B3LYP, Becke-half-and-half-LYP (BHLYP), and QCISD(T) levels of theory along with a polarized double-ζ basis on C and H and the Hay-Wadt relativistic ECP with valence electrons added for the metals. For metal methyl cations, the symmetries were constrained to C_{3v}. It was determined that for first-row MCH_3^+ species (M = Sc–Cu) the B3LYP functional overbinds, with a mean absolute deviation (MAD) from experiment of 0.41 eV. Better estimates are calculated using the BHYLP functional and the QCISD(T) methods, with MADs of 0.18 and 0.20 eV, respectively. For third-row elements, the BDEs calculated using B3LYP were again higher than those obtained using BHLYP and QCISD(T). In contrast, the second study finds that BDEs calculated for metal methylene cations using the BHLYP functional gave estimates below experimental values, whereas those calculated with the B3LYP functional were comparable. Also, these authors concluded that the results were dependent upon the basis set used for the metal ion with an all electron basis yielding more accurate results than effective core potential (ECP) methods. Drawing from these results, the present study carried out calculations for various product ions using the BHLYP functional and QCISD(T)//B3LYP method and the Stuttgart-Dresden (SD) ECP [39] for Hf^+ in addition to the B3LYP/HW + results. Calculations of this sort will be indicated explicitly, otherwise, the calculations have been performed at the B3LYP/HW+/6–311 ++ G (3*df*,3*p*) level of theory.

We calculate a ^{2}D ground state for Hf^+ using the HW^+ basis set and B3LYP level of theory, with a quartet state at 0.298 eV. Using B3LYP/SD, BHLYP/HW^+, and BHLYP/SD combinations of functional and basis sets, the quartet excitation energies are 0.281, 0.283, and 0.239 eV, demonstrating that atomic excitation energies are essentially independent of the basis set and DFT method used. These values are somewhat lower than the 0.563 eV experimental excitation energy between properly weighted spin–orbit levels of the ^{2}D ($6s^25d^1$) and ^{4}F ($6s^15d^2$) states [11]. At the QCISD(T)/HW^+ level of theory, we calculate an excitation energy of 0.774 eV, somewhat above the experimental value.

For calculations of the potential energy surfaces, the B3LYP/HW+/6–311 + G(3*df*,3*p*) level of theory was used. Transition states were located using the synchronous transit-guided quasi-Newton method (QST2 and QST3) [40,41], followed by geometry optimizations and frequency calculations to verify a first order saddle point and IRC calculations or relaxed potential energy surface scans to verify that the transition state connects the appropriate intermediates. For multiply bound species, the B3LYP level of theory does an adequate job of estimating energetics, providing for a high-quality characterization of the overall surface.

3. Experimental results

Fig. 1 shows cross sections for the reaction of CH_4 with Hf^+, which yields products listed in reactions (2)–(5).

$$Hf^+ + CH_4 \rightarrow HfH^+ + CH_3 \quad (2)$$

$$\rightarrow HfCH^+ + H_2 + H \quad (3)$$

$$\rightarrow HfCH_2{}^+ + H_2 \quad (4)$$

$$\rightarrow HfCH_3{}^+ + H \quad (5)$$

We also looked for the HfC^+ product, but its cross section could not be resolved from that of $HfCH^+$, indicating it must be at least an order of magnitude smaller. Cross sections for reactions (3) and (5) have been corrected for mass overlap with the much more intense $HfCH_2{}^+$ cross section. The deuterated analogue of this system yields similar results with less mass overlap, providing for better measurement of product intensities over a broader energy range (Fig. 2).

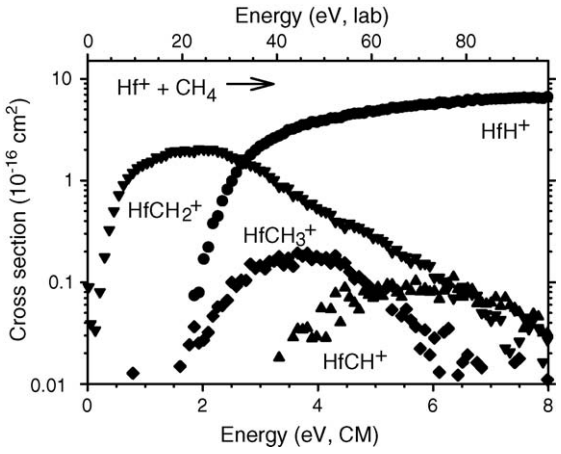

Fig. 1. Cross sections for reaction of Hf^+ (^2D) with CH_4 as a function of kinetic energy in the laboratory (upper *x*-axis) and center of mass (lower *x*-axis) frames.

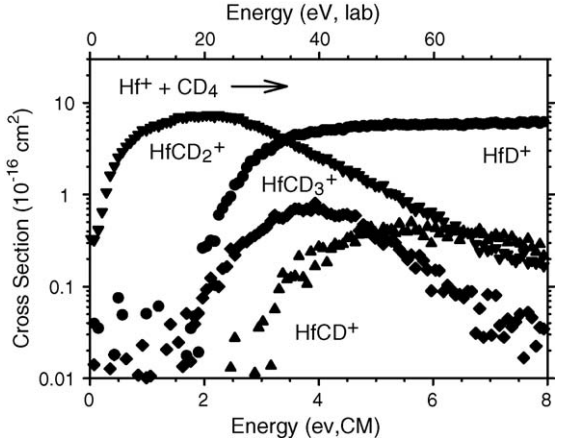

Fig. 2. Cross sections for reaction of Hf^+ (^2D) with CD_4 as a function of kinetic energy in the laboratory (upper *x*-axis) and center of mass (lower *x*-axis) frames.

As illustrated in Figs. 1 and 2, all reactions with methane are endothermic. This is in agreement with previous FTICR studies done by Irikura and Beauchamp who observed no reaction at thermal energy with ground state ions [4]. As the kinetic energy is raised, dehydrogenation of methane to form $HfCH_2^+$ (reaction (4)), is the only process observed at low energies. At higher energies, there is a marked decline in the cross section for $HfCH_2^+$ that correlates with the apparent thresholds for the other products. Only the cross section for HfH^+ is substantial enough to account for the initial drop in intensity of $HfCH_2^+$. Because decomposition of $HfCH_2^+$ to $HfH^+ + CH$ cannot occur until much higher energies, the cross sections must be coupled by competition between reactions (2) and (4), which implies that the two product channels share a common intermediate.

Figs. 1 and 2 show that reactions (2) and (5) and their deuterated analogues have similar apparent thresholds of about 1.5 eV, suggesting that the single bonds for HfH^+ and $HfCH_3^+$ are comparable in strength. Notwithstanding their similar bond strengths, the HfH^+ cross section is more prevalent up to about 4 eV by a factor of about 3.5. Similarly, for the CD_4 system, the HfD^+ cross section exceeds that for $HfCD_3^+$ up to about 4 eV by a factor of about 2. This preference can be attributed largely to angular momentum effects, as discussed further below. Above 4 eV, the $HfCH_3^+$ ($HfCD_3^+$) cross sections decline, which can be attributed partly to subsequent dehydrogenation to form $HfCH^+$ ($HfCD^+$) (reaction (3)). In addition, we find that the sums of the $HfCH_3^+$ and $HfCH^+$ ($HfCD_3^+$ and $HfCD^+$) cross sections also decline above 4 eV. This indicates that dissociation of $HfCH_3^+$ to $Hf^+ + CH_3$, which can begin at 4.48 eV = D(H–CH_3), must also be occurring.

4. Thermochemical and theoretical results

Data analysis of the cross sections is performed using Eq. (1). The optimal parameters for each product cross-section for the CH_4 and CD_4 systems are listed in Table 1. Because all sources of rotational, vibrational, and translational energy are included in the modeling, the E_0 thresholds correspond to 0 K values. The BDEs at 0 K of the hafnium-ligand cations are calculated using Eq. (6):

$$D_0(\mathrm{Hf}^+ - L) = D_0(R - L) - E_0 \quad (6)$$

where $D_0(R-L)$ values can be calculated from heats of formation listed elsewhere [18]. It is assumed that there are no activation barriers other than the endothermicity of the reaction, which is generally the case for ion-molecule reactions because of the long-range attractive forces [25]. The potential energy surfaces calculated here verify this assumption in all cases.

In the following sections, details of our calculations for the products observed in reactions (2)–(5) are discussed. Energetics of these species are provided in Table 2, while Table 3 gives all structural information. BDEs for the likely ground states of the product ions calculated at several levels of theory are compared with experimental values in Table 4.

Table 1
Optimized parameters for Eq. (1) for $Hf^+ + CH_4$ and CD_4 systems

Reaction		σ_0	n	E_0 (eV)	$D_0(Hf^+–L)$ (eV)
$Hf^+ + CH_4$	$\rightarrow HfH^+ + CH_3$	9.05 ± 0.57	0.9 ± 0.1	2.51 ± 0.13	1.97 ± 0.13
	$\rightarrow HfCH_3^+ + H$	0.47 ± 0.08	0.8 ± 0.2	2.38 ± 0.34	2.10 ± 0.34
	$\rightarrow HfCH_2^+ + H_2$	2.54 ± 0.15	1.0 ± 0.1	0.44 ± 0.04	4.27 ± 0.05
	$\rightarrow HfCH^+ + H_2 + H$	0.48 ± 0.16	0.5 ± 0.3	3.96 ± 0.04	5.11 ± 0.16
$Hf^+ + CD_4$	$\rightarrow HfD^+ + CD_3$	18.2 ± 6.1	0.9 ± 0.2	2.60 ± 0.22	1.98 ± 0.22
	$\rightarrow HfCD_3^+ + D$	0.62 ± 0.27	0.9 ± 0.4	2.43 ± 0.41	2.15 ± 0.41
	$\rightarrow HfCD_2^+ + D_2$	10.5 ± 1.8	1.2 ± 0.1	0.33 ± 0.04	4.49 ± 0.05
	$\rightarrow HfCD^+ + D_2 + D$	2.32 ± 0.70	0.7 ± 0.3	4.16 ± 0.39	5.08 ± 0.39

Table 2
B3LYP/HW+/6–311++G(3*df*,3*p*) theoretical energies of reactants and products[a]

Species	State	Energy (E_h)	Zero point energy (E_h)[b]	E_{rel} (eV)[c]
H	^2S	−0.502257		
H_2	$^1\Sigma_g^+$	−1.180030	0.009953	
C	^3P	−37.857442		
CH	$^2\Pi$	−38.495898	0.006457	0.000
	$^4\Sigma^-$	−38.462172	0.006943	0.931
CH_2	$^3B_1$	−39.167949	0.017169	
CH_3	$^2A''$	−39.857664	0.029685	
CH_4	$^1A_1$	−40.536527	0.044503	
Hf^+	^2D	−48.497337		0.000
	^4F	−48.486389		0.298
	^4F	−48.420002		2.104
HfH^+	$^3\Delta$	−49.103320	0.004206	0.000
	$^1\Sigma^+$	−49.098748	0.004404	0.130
	$^3\Pi$	−49.087363	0.004146	0.433
	$^1\Pi$	−49.083655	0.004101	0.533
	$^1\Delta$	−49.081523	0.004177	0.593
	$^3\Phi$	−49.062292	0.003889	1.108
	$^3\Sigma^-$	−49.051891	0.003801	1.389
	$^1\Phi$	−49.050365	0.003931	1.434
	$^1\Gamma$	−49.032709	0.004000	1.916
	$^1\Delta$	−49.009065	0.003896	2.556
$HfCH^+$	$^1\Sigma^+$	−87.177045	0.012765	0.000
	$^3\Pi$	−87.172769	0.012193	0.101
	$^3\Sigma^-$	−87.144439	0.011391	0.850
	$^3\Phi$	−87.137549	0.011915	1.052
$HHfC^+$	$^3A''$	−87.083378	0.007112	0.000 (2.397)
	$^5A''$	−87.076890	0.006601	0.163 (2.559)
	$^1A''$	−87.072754	0.007139	0.290 (2.686)
	$^1\Sigma^+$ ($^1A'$)	−87.061085	0.007319	0.612 (3.009)
	$^5A'$	−87.054698	0.006373	0.761 (3.157)
	$^3A'$	−87.034789	0.006315	1.301 (3.650)
$HfCH_2^+$	$^2A'$	−87.831733	0.021110	0.000
	$^2A_1$ (TS)	−87.829865	0.020314 (−204)	0.029
	$^2B_1$	−87.812945	0.020928	0.506
	$^4B_2$	−87.805013	0.021014	0.725
	$^4B_1$	−87.804947	0.020981	0.729
	$^2A_2$	−87.795142	0.020350	0.975
	$^2B_2$	−87.783332	0.021072	1.316
	$^4A_2$	−87.783319	0.021463	1.327
	$^4A_1$	−87.751197	0.021389	2.199
	$^2A_1$	−87.707169	0.021202	3.392
	$^4B_2$	−87.700530	0.031172	3.572
$HHfCH^+$	$^2A'$	−87.778978	0.017208	0.000 (1.331)
	$^2A''$	−87.769437	0.017334	0.263 (1.594)
	$^4A''$	−87.758773	0.016296	0.542 (1.873)
	$^4A'$	−87.735361	0.016081	1.157 (2.488)
$HfCH_3^+$	$^1A_1$[d]	−88.471146	0.032216	0.000
	^3E	−88.468572	0.032626	0.081
	$^3A_2$	−88.420339	0.033072	1.406
	$^3A_1$	−88.368018	0.031424	2.785
$HHfCH_2^+$	$^1A'$	−88.440676	0.027891	0.000 (0.713)
	$^1A'$	−88.438185	0.026881	0.041 (0.753)
	$^3A''$	−88.420940	0.026377	0.496 (1.209)
$(H)_2HfCH^+$	$^3A''$	−88.372489	0.022808	0.000 (2.432)
	$^1A_1$	−88.336447	0.023116	0.989 (3.420)
$(H_2)HfCH^+$	$^3A''$	−88.372573	0.027327	0.000 (2.551)
	$^1A''$	−88.369166	0.027269	0.091 (2.642)
	$^3A'$	−88.349986	0.026283	0.587 (3.138)
	$^1A_1$	−88.290278	0.023683	2.141 (4.692)

[a] All species exhibit s(s + 1) values in agreement with the spin states shown (0.0 for singlet, 0.75 for doublet, 2.00 for triplet, and 3.75 for quartet) with the following exceptions: Hf^+(^2D), s(s + 1) = 1.28; $HfCH_2^+$ ($^2B_1$), s(s + 1) = 1.37; and $HfCH_2^+$ ($^2B_2$), s(s + 1) = 1.75. For Hf^+ (^2D, $6s^25d^1$), an energy of $-48.4900274E_h$ (E_{rel} = 0.199 eV) is found for a level having no spin contamination.
[b] Imaginary frequencies (cm^{-1}) in parentheses.
[c] Energy relative to the ground state species including zero point energies scaled by 0.989. Values in parentheses are relative to the lowest energy isomer.
[d] A spin contaminated, s(s + 1) = 0.63, version of this state was also located at $-88.476363E_h$.

4.1. HfH^+

The bond energy of Hf^+–H has recently been measured from the reaction of Hf^+ with H_2 and D_2, yielding an average value of 2.07 ± 0.09 eV [42]. From Eq. (6) with $D_0(CH_4)$ = 4.48 eV and our threshold of 2.51 ± 0.13 eV (Table 1), we obtain a BDE for HfH^+ of 1.97 ± 0.13 eV, within experimental uncertainty of the previous thermochemistry. Similarly, with $D_0(CD_4)$ = 4.58 eV, a threshold of 2.60 ± 0.22 eV, and a calculated zero point energy difference between HfD^+ and HfH^+ of 0.033 eV, the BDE derived from the CD_4 system for HfH^+ is 1.95 ± 0.22 eV, again in good agreement. Thus, the CH_4 and CD_4 systems behave similarly to each other and agree nicely with the thermodynamic results for the H_2 and D_2 systems. On average, the BDE obtained from the methane systems is lower by 0.10 ± 0.13 eV, a minor discrepancy that may be attributed to a competitive shift with the lower energy dehydrogenation reaction.

Ohanessian et al. calculate that the ground state for HfH^+ is $^3\Delta$ where the character of the bonding orbital on Hf is 35% 6*s* and 64% 5*d* [36]. This bonding can be thought of as stemming from a covalent bond between the 1*s* orbital on H and a 6*s*5*d* hybrid orbital on Hf^+. This type of hybridization is quite efficient in the third-row transition metals because of the relativistic effects involved, making the 6*s* orbital comparable in size to the 5*d* orbitals. Such a singly occupied 6*s*5*d* orbital is formed by a combination of the ^2D ($6s^25d^1$) and ^4F ($6s^15d^2$) states. Consequently, even though binding to the hybrid orbital of Hf^+ requires both promotion and the loss of exchange energy because the ^4F state configuration is mixed in, the 6*s*5*d* hybrid bonding orbital overlaps better with the 1*s* orbital on H(^2S) than pure 6*s* or 5*d* orbitals. The nonbonding valence orbitals that are occupied in the $^3\Delta$ state are $\sigma^1\delta^1$, where the σ orbital is largely 6*s* and the δ orbital is pure 5*d*. The bond length calculated by Ohanessian et al. is 1.79 Å [36], which is in good agreement with the bond length calculated here of 1.79 Å. We also calculated results for stable excited states (with nonbonding valence occupancies) of $^1\Sigma^+(\sigma^2)$, $^3\Pi(\sigma^1\pi^1)$, $^1\Pi(\sigma^1\pi^1)$, $^1\Delta(\sigma^1\delta^1)$, $^1\Gamma(\delta^2)$, $^3\Phi(\pi^1\delta^1)$, $^3\Sigma^-(\pi^2, \delta^2)$, $^1\Phi(\pi^1\delta^1)$, and $^1\Delta(\pi^2)$, with relative energies listed in Table 2 and geometries in Table 3. Note that

Table 3
B3LYP/HW+/6–311++G(3*df*,3*p*) theoretical structures of reactants and products[a]

Species	State	*r*(Hf—H)	*r*(Hf—C)	*r*(C—H)	∠HfCH	∠HCH	∠Dihedral[b]
CH	$^2\Pi$			1.122			
	$^4\Sigma^-$			1.093			
CH_2	$^3B_1$			1.078(2)		135.1	
CH_3	$^2A''$			1.078(3)		120.0(3)	180.0
CH_4	$^1A_1$			1.088(4)		109.5(6)	120.0(6)
HfH^+	$^3\Delta$	1.786					
	$^1\Sigma^+$	1.746					
	$^3\Pi$	1.776					
	$^1\Pi$	1.781					
	$^1\Delta$	1.787					
	$^3\Phi$	1.826					
	$^3\Sigma^-$	1.824					
	$^1\Phi$	1.821					
	$^1\Gamma$	1.824					
	$^1\Delta$	1.814					
$HfCH^+$	$^1\Sigma^+$		1.801	1.085	180.0		
	$^3\Pi$		1.896	1.086	180.0		
	$^3\Sigma^-$		2.036	1.088	180.0		
	$^3\Phi$		1.916	1.085	180.0		
$HHfC^+$	$^3A''$	1.792	1.909		96.9[c]		
	$^5A''$	1.783	2.084		98.5[c]		
	$^1A''$	1.792	1.906		96.9[c]		
	$^1\Sigma^+$ ($^1A'$)	1.817	1.795		180.0[c]		
	$^5A'$	1.803	2.102		107.2[c]		
	$^3A'$	1.779	2.260		95.4[c]		
$HfCH_2^+$	$^2A'$		1.883	1.082, 1.130	86.6, 161.0	112.4	180.0
	$^2A_1$ (TS)		1.915	1.093(2)	123.2(2)	113.5	180.0
	$^2B_1$		2.080	1.092(2)	123.6(2)	112.8	180.0
	$^4B_2$		2.103	1.091(2)	123.7(2)	112.6	180.0
	$^4B_1$		2.102	1.091(2)	123.7(2)	112.7	180.0
	$^2A_2$		1.940	1.092(2)	123.4(2)	113.2	180.0
	$^2B_2$		2.103	1.091(2)	123.7(2)	112.6	180.0
	$^4A_2$		2.124	1.092(2)	124.6(2)	110.8	180.0
	$^4A_1$		2.160	1.091(2)	124.4(2)	111.2	180.0
	$^2A_1$		2.445	1.097(2)	125.0(2)	110.0	180.0
	$^4B_2$		2.485	1.098(2)	126.0(2)	108.1	180.0
$HHfCH^+$	$^2A'$	1.801	1.904	1.086	97.4,[c] 176.0		0.0
	$^2A''$	1.797	1.904	1.085	97.0,[c] 174.0		0.0
	$^4A''$	1.785	2.063	1.087	98.9,[c] 176.8		0.0
	$^4A'$	1.805	2.080	1.086	105.8,[c] 176.5		0.0
$HfCH_3^+$	$^1A_1$		2.072	1.096(3)	109.2(3)	109.7(3)	120.0(3)
	^3E		2.120	1.096(3)	109.5(3)	109.4(3)	120.0(3)
	$^3A_2$		2.194	1.095(3)	109.7(3)	109.3(3)	120.0(3)
	$^3A_1$		2.229	1.098(3)	111.3(3)	107.6(3)	120.0(3)
$HHfCH_2^+$	$^1A'$	1.803	1.889	1.083, 1.131	85.2, 98.5,[c] 162.3,	112.5	0.0, 180.0
	$^1A'$	1.803	1.902	1.083, 1.116	97.0, 98.8,[c] 149.8,	113.2	0.0, 180.0
	$^3A''$	1.788	2.095	1.091, 1.092	100.7,[c] 120.8, 126.8	112.4	0.0, 180.0
$(H)_2HfCH^+$	$^3A''$	1.785(2)	2.066	1.087	99.0(2),[c] 175.7	101.0[d]	±51.4
	$^1A_1$	1.809(2)	2.031	1.089	121.9(2),[c] 180.0	116.3[d]	0.0(2)
$(H_2)HfCH^+$	$^3A''$	2.026, 2.056	1.926	1.086	68.5,[c] 91.6,[c] 179.8	23.1[d]	0.0(2)
	$^1A''$	2.028, 2.056	1.929	1.086	69.0,[c] 92.1,[c] 179.9	23.1[d]	0.0(2)
	$^3A'$	1.971, 1.996	1.941	1.086	66.4,[c] 90.6,[c] 179.7	24.1[d]	180.0(2)
	$^1A_1$	2.538(2)	2.063	1.088	171.5(2),[c] 180.0	17.1[d]	0.0, 180.0

[a] Bond lengths are in Å. Bond angles are in degrees. Degeneracies are listed in parentheses.
[b] Generally, ∠HHfCH except for the CH_x species where it is ∠HCHH.
[c] ∠HHfC.
[d] ∠HHfH.

Table 4
Experimental and theoretical bond energies for Hf^+—H and Hf^+—CH_x ($x = 1$–3)[a]

Species	State	Exp	B3LYP		BHYLP		QCISD(T)[b]
			HW+	SD	HW+	SD	HW+
Hf^+—H	$^3\Delta$[c]	2.07 ± 0.09	2.71 (2.44)	2.63 (2.35)	2.59 (2.31)	2.54 (2.22)	2.34 (2.55)
	$^1\Sigma^+$		2.58	2.44	2.42	2.30	2.74
Hf^+—CH_3	$^1A_1$	2.12 ± 0.26	3.09	2.88	2.76	2.57	3.54
	^3E[c]		3.01 (2.74)	2.87 (2.59)	2.73 (2.45)	2.63 (2.31)	2.93 (3.14)
Hf^+—CH_2	$^2A'$	4.37 ± 0.07	4.42	4.21	3.85	3.66	4.56
Hf^+—CH	$^1\Sigma^+$	5.10 ± 0.15	4.83	4.63	4.13	3.97	4.97

[a] All theoretical values may need to be decreased by the average spin-orbit energy of the Hf^+ (^2D) state, 0.227 eV [11], in which case corrections for the spin-orbit levels of the HfH^+ and $HfCH_x^+$ species would also be needed, but these are unknown.
[b] Geometries calculated at the B3LYP/HW+ level of theory.
[c] Values in parentheses are referenced to the Hf^+ (^4F) asymptote and adjusted by the experimental excitation energy for this state, 0.563 eV [11].

the excitation energy of the $^1\Sigma^+$ state (0.13 eV) is sufficiently low that there is the possibility that this is the true ground state. This state is relatively low in energy because it can be formed directly from the Hf^+ (^2D, $6s^25d^1$) state (thereby avoiding promotion and exchange energy costs) by coupling the H(1*s*) electron with the 5*d* electron. Ohanessian et al. examined the triplet excited states (but no singlet states) finding the $^3\Pi(\sigma^1\pi^1)$ at 0.49 eV, a $^3\Phi(\pi^1\delta^1)$ at 1.01 eV, and the $^3\Sigma^-(\pi^2, \delta^2)$ at 1.10 eV, all with bond lengths comparable to the present calculations [36].

As noted above, the $^1\Sigma^+$ state is only 0.13 eV above the $^3\Delta$ state at the B3LYP/HW+ level of theory. Other levels of theory agree that the $^3\Delta$ state is the ground state, with excitation energies for the $^1\Sigma^+$ state of 0.19 (B3LYP/SD), 0.17 (BHLYP/HW+), and 0.24 (BHLYP/SD) eV. However, at the QCISD(T)/HW+//B3LYP/HW+ level of theory, the $^1\Sigma^+$ is calculated to have a BDE of 2.74 eV, 0.40 eV more than the $^3\Delta$ state. Complicating the assignment of the true ground state is the fact that whereas the $^1\Sigma^+$ state can be derived from pure Hf^+ (^2D), the $^1\Delta$ state mixes in Hf^+ (^4F) character such that errors in the excitation energy of this state (see above) may propagate to the relative energies of the $^3\Delta$ and $^1\Sigma^+$ states. Indeed if the errors in the ^4F excitation energies noted above are included in full (yielding the BDEs listed in parentheses in Table 4), the $^1\Sigma^+$ state becomes the ground state in all cases, with $^3\Delta$ excitation energies of 0.14, 0.09, 0.11, 0.08, and 0.19 eV for the B3LYP/HW+, B3LYP/SD, BHLYP/HW+, BHLYP/SD, and QCISD(T)/HW+ calculations, respectively (Table 4).

Ohanessian et al. calculated a BDE for the $^3\Delta$ state of HfH^+ of 2.38 eV using generalized valence bond theory (GVB) [36], a value somewhat above our experimental BDE. Theoretical BDEs for this state calculated here at all levels of theory greatly exceed the experimental BDE if the values are referenced to the Hf^+ (^2D) state. If referenced to the ^4F state of Hf^+ and corrected by the experimental excitation energy, the $^3\Delta$ is no longer the ground state (see above) (Table 4). Likewise the BDEs calculated for the $^1\Sigma^+$ state exceed the experimental value at all levels of theory. One possible reason for the discrepancy is to realize that the calculations are referenced to the average of the spin–orbit levels of Hf^+ (^2D), which experimentally lies 0.227 eV above the $^2D_{3/2}$ level, the experimental ground level [11]. If the BDEs for the $^1\Sigma^+$ state in Table 4 are reduced by this amount, it can be seen that the BHLYP values agree with experiment within the uncertainties, 2.19 (HW+) and 2.07 (SD) eV compared to 2.07 ± 0.09 eV. The B3LYP values remain high even with this correction, 2.35 (HW+) and 2.21 (SD) eV, consistent with the observations of Holthausen et al. for metal–ligand single bonds [37].

4.2. $HfCH_3^+$

The BDE of Hf^+–CH_3 derived from the CH_4 system is 2.10 ± 0.34 eV and the BDE of Hf^+–CD_3 derived from the CD_4 system is 2.15 ± 0.41 eV (Table 1). After correcting for the zero point energy differences in these two values (0.012 eV), their weighted average is 2.12 ± 0.26 eV for the BDE of Hf^+–CH_3. This value is similar to the value obtained for HfH^+, $D_0 = 2.07 \pm 0.09$ eV, as expected for a single covalent bond to Hf^+.

The experimental BDE derived for $HfCH_3^+$ can be compared to calculations made by Holthausen et al., who have performed studies on first- and third-row transition metal methyl cations [37]. These calculations were performed using the B3LYP, BHLYP, QCISD, and QCISD(T) levels of theory, yielding values for the Hf^+–CH_3 BDEs of 3.10, 2.80, 2.65, and 2.68 eV, respectively. Comparison of the theoretical calculations and experimentally derived values for the first-row transition metal methyl cations leads to an empirical correction for the BHLYP and QCISD(T) methods of −0.22 and +0.16 eV, yielding corrected values of 2.58 and 2.84 eV with estimated errors of ±0.22 eV. All these values are well above our experimental value of 2.12 ± 0.26 eV.

Our calculations find that the ground state for $HfCH_3^+$ is $^1A_1$, in which the bonding involves the interaction of the singly occupied sp^3 hybridized orbital on CH_3 and the singly occupied $5d\sigma$ orbital on Hf^+ (^2D, $6s^25d^1$). This state, the equivalent of HfH^+ ($^1\Sigma^+$), requires no promotion energy or loss of exchange energy for binding to Hf^+ (^2D). The two nonbonding valence electrons in this state occupy an a_1 orbital that is essentially the 6*s* orbital of Hf hybridized with some 5*d* character. The equivalent of the HfH^+ ($^3\Delta$) ground state is now the ^3E ($a_1^1e^1$), which lies only 0.08 eV higher in energy and therefore could be the true ground state. The switch in the ground state character

between the HfH^+ and $HfCH_3^+$ molecules indicates the subtle nature of the hybridization and promotion energies in these systems. Indeed, in their calculations, Holthausen et al. report that $HfCH_3^+$ has a ^3E state, although it is unclear whether a singlet state was explicitly considered [37]. Our calculated bond length for Hf–C is 2.07 Å in the $^1A_1$ state and 2.12 Å in the ^3E state, where the latter value is in good agreement with the bond length of 2.11 Å calculated by Holthausen et al. at the QCISD(T) level [37]. We also calculated energies for stable excited states (with nonbonding valence occupancies) of $^3A_2$ (e^2) and $^3A_1$ ($a_1^1a_1^1$), with relative energies listed in Table 2 and geometries in Table 3. (The $^3A_2$ state is misidentified in the Gaussian code as $^3A_1$. As discussed elsewhere [43], the properly antisymmetrized wavefunctions for an (e^2) configuration lead to $^1A_1$, ^1E, and $^3A_2$ states.)

As noted above, the excitation energy for the ^3E state at the B3LYP/HW$^+$ level of theory is only 0.08 eV. B3LYP/SD, BHLYP/HW+, and QCISD(T)/HW+//B3LYP/HW+ levels of theory also find a $^1A_1$ ground state, with ^3E state excitation energies of 0.01, 0.03, and 0.61 eV, respectively. The BHLYP/SD combination reverses the order of the states such that the ^3E state has a BDE of 2.63 eV, with an excitation energy for the $^1A_1$ state of 0.06 eV. If the BDEs of the triplet state are referenced to the Hf^+ (^4F) asymptote instead and then corrected by the experimental excitation energy of this state, the BDEs fall to 2.74, 2.59, 2.45, 2.31, and 3.14 eV, respectively (Table 4).

For our B3LYP/HW$^+$ theoretical calculations, we obtain $D_0(Hf^+–CH_3) = 3.09$ eV for the $^1A_1$ state and 3.01 eV for the ^3E state. The latter value compares favorably with the B3LYP calculations made by Holthausen et al., $D_0 = 3.03$ eV [37]. Using the SD ECP on Hf^+, a value of 2.88 eV was obtained for the $^1A_1$ state. Again, to offset the overbinding of the B3LYP functional for single covalent metal–ligand bonds, we carried out calculations using the BHLYP functional to provide a better estimate of $D_0(Hf^+–CH_3, {}^1A_1)$. Using this level of theory, we obtain lower values of 2.76 (HW+) and 2.57 (SD) eV, which are in better agreement but still exceed our experimental value of 2.12 ± 0.26 eV. If these values are corrected for the 0.227 eV average spin–orbit state implicit in the theoretical calculations (see discussion above), the agreement is better, 2.53 and 2.34 eV, respectively. Our BHLYP/HW+ value for the ^3E state of 2.73 eV matches the BHLYP value from Holthausen et al. of $D_0 = 2.72$ eV [37]. At the QCISD(T) level of theory, we calculate a BDE of 3.54 eV for $D_0(Hf^+–CH_3, {}^1A_1)$ and 2.93 eV for the ^3E state, whereas Holthausen et al. get $D_0 = 2.60$ eV for the latter [37]. In accordance with HfH^+ and $HfCH_3^+$ having similar single covalent metal–ligand bonds and similar experimental BDEs, theoretical results obtained for these two species are comparable with one another.

We also examined alternate isomers of $HfCH_3^+$, namely $HHfCH_2^+$ and $(H)_2HfCH^+$. The lowest-lying hafnium hydrido methylidene isomer has a $^1A'$ state and lies 0.71 eV above the hafnium methyl isomer. This planar molecule has Hf–H and Hf–C bond lengths comparable to those of HfH^+ and $HfCH_2^+$, with a HHfC bond angle of 99° (Table 3). The triplet state of this isomer is similar in structure but has an elongated Hf–C bond. The hafnium dihydride methylidyne structure is still higher in energy, 2.43 eV, and has a triplet as its lowest energy state. This species has Hf–H bond lengths characteristic of HfH^+ ($^3\Delta$), but the HfC bond is quite long, 2.07 Å compared to 1.90 Å for $HfCH^+$ ($^3\Pi$). The three covalent bonds in this molecule are essentially perpendicular to one another, indicating the use of 5*d* orbitals for bonding on Hf. Notably, several calculations of $(H)_2HfCH^+$ species collapsed to a $(H_2)HfCH^+$ geometry in which dihydrogen is electrostatically bound to $HfCH^+$. The lowest of these isomers is a $^3A''$, lying 2.55 eV above the $HfCH_3^+$ ground state (Table 2).

4.3. $HfCH_2^+$

The thresholds for dehydrogenation (reaction (4)), in the CH_4 and CD_4 systems are 0.44 ± 0.04 and 0.33 ± 0.04 eV. Combined with a ZPE correction of 0.015 eV, these results yield BDEs for $Hf^+–CH_2$ derived from the CH_4 and CD_4 systems of 4.27 ± 0.05 and 4.47 ± 0.05 eV, respectively. The weighted mean for these two values of $D_0(Hf^+–CH_2)$ is 4.37 ± 0.07 eV. This value is in good agreement with the results of Irikura and Beauchamp [4] who determined that $4.0\,\text{eV} < D_0(Hf^+–CH_2) < 4.8$ eV using FTICR mass spectrometry. These limits were obtained by bracketing the formation of $HfCH_2^+$ in reactions of Hf^+ with cyclopropane, which is exothermic, and that with methane, which is endothermic. Irikura and Goddard calculated a bond energy (D_e) of 3.99 eV, but empirically correct this by 0.52 eV to yield a recommended bond energy (D_0) of 4.51 ± 0.22 eV [44]. For our B3LYP theoretical calculations, we obtain BDEs for $Hf^+–CH_2$ of 4.42 (HW+) and 4.21 (SD) eV, which are in good agreement with our experimental results. At the BHYLP level of theory, we calculate values of 3.85 (HW+) and 3.66 (SD) eV for $D_0(Hf^+–CH_2)$, which are below the experimental results. At the QCISD(T) level of theory, a value of 4.56 eV for $D_0(Hf^+–CH_2)$ was obtained, slightly higher than experiment.

The ground state of $HfCH_2^+$ was found to be $^2A'$, whereas Irikura and Goddard reported a $^2A_1$ ground state because they constrained their GVB calculations to C_{2v} symmetry [44]. Indeed, we find that this $^2A_1$ state is a transition state that lies 0.029 eV (0.051 eV before zero point energy corrections) above the ground state of the hafnium methylidene cation. The imaginary frequency of 204 cm^{-1} corresponds to an in-plane, wagging motion that leads to the distorted $^2A'$ ground state. Because the zero point energy of this molecule (0.57 eV) is much greater than the barrier, the hafnium methylidene cation effectively has C_{2v} symmetry. Our calculations find that the $^2A_1$ state has r(Hf–C) = 1.92 Å, r(C–H) = 1.09 Å and ∠HfCH = 123°, whereas the GVB results find values of 2.00 Å, 1.09 Å, and 123°, respectively. The electronic configuration is $(1a_{1b})^2(1b_{1b})^2(2a_1)^1$, where the $1a_{1b}$ and $1b_{1b}$ orbitals are the Hf–C σ and π bonding orbitals. Nonbonding orbitals on the hafnium include the $2a_1$ ($6s$–$5d_{z2}$), $3a_l$ ($5d_{x2-y2}$), $1a_2$ ($5d_{xy}$), and $1b_2$ ($5d_{yz}$) given that the molecule lies in the *yz*-plane with the Hf–C bond along the *z*-axis [44]. Excited states identified by Irikura and Goddard include $^2A_2$ $[(1a_{1b})^2(1b_{1b})^2(1a_2)^1]$ and $^4A_1$ $[(1a_{1b})^2(1b_{1b})^1(2a_1)^1(2b_1{}^*)]$ lying 0.97 and 1.47 eV, respectively, above the ground state. Our calculations find

excited states of $^2B_1[(1a_{1b})^2(1b_{1b})^1(2a_1)^2]$, $^4B_2[(1a_{1b})^2(1b_{1b})^1(2a_1)^1(1a_2)^1]$, $^4B_1[(1a_{1b})^2(1b_{1b})^1(2a_1)^1(3a_1)^1]$, $^2A_2[(1a_{1b})^2(1b_{1b})^2(1a_2)^1]$, $^2B_2[(1a_{1b})^2(1b_{1b})^1(2a_1)^1(1a_2)^1]$, $^4A_2[(1a_{1b})^2(1b_{1b})^1(2a_1)^1(1b_2)^1]$, $^4A_1[(1a_{1b})^2(1b_{1b})^1(1a_2)^1(1b_2)^1]$, $^2A_1[(1a_{1b})^2(2a_1)^2(3a_1)^1]$, and $^4B_2[(1a_{1b})^2(2a_1)^1(3a_1)^1(1b_2)^1]$, with relative energies listed in Table 2 and geometries in Table 3. Note that our excitation energy for the $^2A_2$ state agrees well with that of Irikura and Goddard, but that we find a lower-lying doublet state at 0.51 eV, $^2B_1$, as well as a lower-lying quartet state at 0.72 eV, $^4B_2$.

We also examined the alternate isomer of $HfCH_2^+$, namely $HHfCH^+$. The lowest state of this isomer, $^2A'$, lies 1.33 eV above the $HfCH_2^+$ ($^2A'$) ground state. In all cases, the HfCH part of the molecule is nearly linear (bond angles of ∼175°, Table 3), whereas the HHfC bond angle is close to 100°, indicating that 6*s*–5*d* hybrids are used to form the two covalent bonds to Hf. Excited states, $^2A''$, $^4A''$, and $^4A'$, were found lying 1.59, 1.87, and 2.49 eV higher in energy, respectively (Table 2).

4.4. $HfCH^+$

Experimental cross sections for the formation of $HfCH^+$ and $HfCD^+$ were analyzed to yield thresholds of 3.96 ± 0.15 and 4.16 ± 0.39 eV, respectively. This corresponds to BDEs of 5.11 ± 0.16 and 5.08 ± 0.39 eV for the perprotio methane and perdeuterated methane systems. After correcting for a zero-point energy difference in the BDEs of 0.028 eV, we obtain a weighted mean for these two values of $D_0(Hf^+{-}CH) = 5.10 \pm 0.15$ eV. This value is deemed a lower limit to the true thermodynamic value because of the possibility of competition with other channels.

The ground state configuration of $HfCH^+$ is calculated to be $^1\Sigma^+$, having a $1\sigma_b^2 1\pi_b^4$ valence electron configuration in which a triple bond is formed between hafnium and carbon. For our theoretical calculations, we obtain $D_0(Hf^+{-}CH)$ of 4.83 (HW+) and 4.63 (SD) eV using B3LYP, somewhat below experiment. Using BHLYP, values are 4.13 (HW+) and 3.97 (SD) eV, which are well below the experimental results. At the QCISD(T) level of theory, we calculate a value of 4.97 eV for $D_0(Hf^+{-}CH)$, in reasonable agreement with experiment. Irikura and Goddard estimated a much higher value for $D_0(Hf^+{-}CH)$ of 6.2 eV, derived from an intrinsic bond energy model [44] and well above our experimental value. The Hf–C bond length and HfCH bond angle (Table 3) in the ground state are calculated to be 1.80 Å and 180°. The lowest lying excited state is $^3\Pi$, which lies 0.10 eV higher in energy and corresponds to excitation of a π-bonding electron into a σ-nonbonding (largely 6*s*) orbital. Thus, the Hf–C bond length increases to 1.90 Å. Other excited states, all with longer Hf–C bond lengths (Table 3), include $^3\Sigma^-$ (0.85 eV, excitation of σ-bonding to σ-nonbonding orbitals) and $^3\Phi$ (1.05 eV, excitation of π-bonding to δ-nonbonding orbitals).

We also examined the alternate isomer of $HfCH^+$, namely $HHfC^+$. In all cases, these species are bent and lie well above the energy of the methylidyne isomer, with the lowest lying state, $^3A''$, being 2.40 eV higher in energy (Table 2).

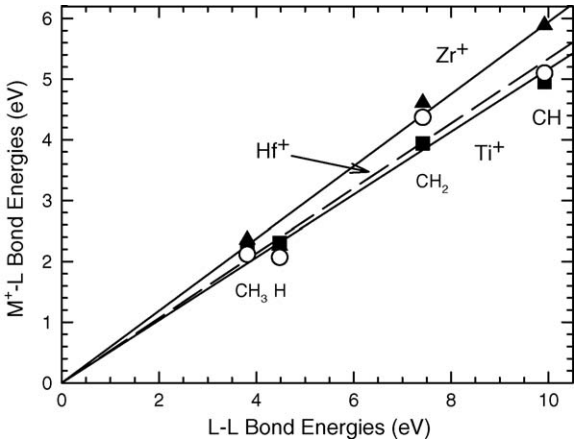

Fig. 3. Correlation of $Hf^+{-}L$ bond energies with those for the organic analogues, L–L. $Hf^+{-}L$ values (open circles) are from Table 4. Data for Ti^+ and Zr^+ are listed in the text and shown by squares and triangles, respectively. The lines are linear regression fits to the experimental data constrained to pass through the origin to emphasize the bond-order correlations.

4.5. Bond-energy bond-order correlation for $Hf^+{-}CH_x$ bonds

One interesting way of investigating the bond order of simple metal–ligand species is to compare with organic analogues, i.e., $D_0(Hf^+{-}L)$ versus $D_0(L{-}L)$. Such a plot is shown in Fig. 3. It can be seen that the correlation is remarkably good, which indicates that $Hf^+{-}H$ and $Hf^+{-}CH_3$ are single bonds, $Hf^+{=}CH_2$ is a double bond, and $Hf^+{\equiv}CH$ is a triple bond, as confirmed by theory. (The linear regression line in Fig. 3 is constrained to include the origin to emphasize the bond-order correlation of HfL^+ versus L_2 species.)

It is also interesting to compare these results to those for the first-row and second-row congeners, Ti^+ and Zr^+ (Fig. 3). BDEs for TiH^+, $TiCH^+$, $TiCH_2^+$, and $TiCH_3^+$ are 2.31 ± 0.11, 4.95 ± 0.05, 3.94 ± 0.09, and 2.22 ± 0.03 eV, respectively [45]. The analogous species for Zr have BDEs of 2.26 ± 0.08, 5.89 ± 0.13, 4.61 ± 0.05, and 2.36 ± 0.10 eV, respectively [19,46]. From this comparison, we find that the first- and second-row transition-metal bonded species of Ti^+ and Zr^+ are quite comparable to those of Hf^+. On average, the linear regression lines indicate that the bonds to Zr^+ are 10% stronger than those to Hf^+, and the multiply bonded Hf species are 8% stronger than those to Ti^+. This is in contrast to most other columns of the periodic table where the lanthanide contraction allows the third-row metals to form much stronger bonds than the first- and second-row congeners [31–34]. This difference in behavior can again be attributed to the unusual doubly occupied $6s^2$ orbital of Hf^+ (^2D).

4.6. Potential energy surfaces of $[Hf,C,4H]^+$

Fig. 4 illustrates the potential energy surfaces (PESs) for the interaction of Hf^+ with methane. The energies of all intermediates are provided in Table 5, while Table 6 shows geometric parameters these species. Our ab initio calculations indicate

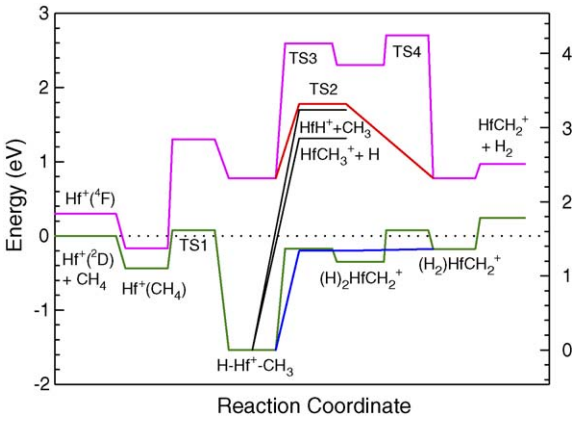

Fig. 4. $[Hf,C,4H]^+$ potential energy surfaces derived from theoretical results. The energies of all species relative to the $Hf^+(^2D)+CH_4$ ground state asymptote are based on ab initio calculations at the B3LYP/HW+/6–311++G(3*df*,3*p*) level (see Table 5). Doublet surfaces are in green (^{2}TS3 and ^{2}TS4) and blue (^{2}TS2). Quartet surfaces are in pink (^{2}TS3 and ^{2}TS4) and red (^{2}TS2).

that the ground states of all intermediates and transition states leading from Hf^+ (^2D) + CH_4 to the $HfCH_2^+$ ($^2A'$) + H_2 ($^1\Sigma_g^+$) products have doublet-spin ground states. Therefore, the dehydrogenation process is spin-allowed. The quartet surface remains higher in energy throughout the entire PES, such that coupling between the doublet and quartet surfaces is anticipated to be unimportant in the observed reactivity. It should also be noted that formation of the HfH^+ ($^3\Delta$, $^1\Sigma^+$)+CH_3 ($^2A''$) and $HfCH_3^+$ ($^1A_1$, ^3E)+H (^2S) products are spin-allowed from doublet intermediates.

4.7. Doublet surface

On the doublet surface, Hf^+ (^2D, $6s^25d^1$) reacts with methane to form an $Hf^+(CH_4)$ adduct in which the methane molecule remains intact and largely unperturbed (Fig. 5). The methane binds with C_s symmetry in a $^2A'$ state and has a Hf–C bond distance of 2.66 Å. This species has a valence electron configuration on the metal that is $(1a')^2(2a')^1$ in which the 1a′ orbital is mostly 6*s* (nearly a_1) and the 2a′ is a $b_2(\pi)$-like orbital with its lobes perpendicular to the plane defined by the H-atoms closest

Table 5
B3LYP/HW+/6–311++G(3*df*,3*p*) theoretical energies of $[Hf,C,4H]^+$ intermediates and transition states

Species	State	$s(s+1)$[a]	Energy (E_h)	Zero point energy (E_h)[b]	E_{rel} (eV)[c]
$Hf^+(^2D)+CH_4$	^2D	1.28*	−89.033864	0.044503	0.000
$Hf^+(CH_4)$	$^2A'$	1.25*	−89.050420	0.045022	−0.437
	^4A	3.75	−89.040310	0.044914	−0.164
	$^4B_2$	3.75	−89.040032	0.046340	−0.118
TS1	^2A	0.75	−89.023674	0.037030 (−1069)	0.076
	^4A	3.75	−88.978257	0.036636 (−445)	1.301
$HHfCH_3^+$	$^2A'$	0.75	−89.084072	0.038104	−1.538
	$^2A''$	0.76	−89.061408	0.038255	−0.918
	$^4A'$	3.76	−88.996956	0.036036	0.776
	$^4A''$	3.76	−88.996978	0.036190	0.780
	$^4A_2$	3.76	−88.955091	0.036632	1.932
TS2	$^2A'$	0.75	−89.032631	0.035860 (−330)	−0.199
	$^4A''$	3.76	−88.958576	0.034456 (−1263)	1.778
TS3	^2A	0.76	−89.028602	0.032822 (−644)	−0.171
	$^4A'$	3.76	−88.921983	0.027837 (−833)	2.596
$(H)_2HfCH_2^+$	$^2A'$	0.75	−89.035591	0.033191	−0.351
	$^4A_1$	3.76	−88.940595	0.029210	2.126
	$^4A''$	3.76	−88.934602	0.029184	2.289
	$^4A_1$	3.76	−88.922959	0.029810	2.622
TS4	^2A	0.75	−89.021080	0.034374 (−553)	0.075
	$^4A'$	3.76	−88.916988	0.026862 (−620)	2.706
$(H_2)HfCH_2^+$	$^2A'$	0.75	−89.032724	0.036813	−0.176
	^2A	0.75	−89.028202	0.037841	−0.025
	$^2A'$	0.75	−89.019558	0.034285	0.114
	$^2A''$	1.40*	−88.998800	0.033158	0.649
	$^4A'$	3.75	−88.995414	0.034566	0.779
	$^4A''$	3.75	−88.995377	0.034851	0.788
	$^4A_2$	3.75	−88.976940	0.036097	1.323
	$^2A_1$	0.75	−88.891713	0.033319	3.567

[a] Values indicating spin contamination are marked with an asterisk.
[b] Imaginary frequencies (cm^{-1}) in parentheses.
[c] Energy relative to the ground state reactants including zero point energies scaled by 0.989.

Table 6
B3LYP/HW+/6–311++G(3*df*,3*p*) theoretical structures of $[Hf,C,4H]^+$ intermediates and transition states[a]

Species	State	*r*(Hf—H)	*r*(Hf—C)	*r*(C—H)	*r*(H—H)	∠HfCH	∠HCH	∠HHfC	∠HHfH	∠HHfCH
$HfCH_4^+$	$^2A'$	2.319(2)	2.665	1.086, 1.090, 1.107(2)		60.0(2), 107.6, 141.0	104.9(2), 110.6(2), 111.3, 114.3			
	^4A	2.247, 2.394	2.699	1.087, 1.088, 1.101, 1.112		54.7, 62.3, 118.3, 129.7	105.5, 106.9, 107.7, 108.9, 111.6, 116.3			
	$^4B_2$	2.293(2)	2.672	1.088(2), 1.108(2)		58.3(2), 124.2(2)	107.2(4), 111.7, 116.6			
TS1	^2A	1.882	2.103	1.091(2), 1.199, 1.395		61.2, 70.6, 124.0, 124.2	101.5(2), 105.2(2), 111.0, 131.8	40.5		
	^4A	1.808	2.549	1.082, 1.085, 1.092		84.7, 102.0, 105.2	117.5, 118.3, 119.2	85.0		
$HHfCH_3^+$	$^2A'$	1.785	2.106	1.097(2), 1.098		108.2, 110.6(2)	109.6, 108.9(2)	100.3		0.0, ±119.2
	$^2A''$	1.802	2.125	1.097(2), 1.098		105.3, 112.4(2)	108.3, 109.2(2)	102.3		0.0, ±118.7
	$^4A'$	1.868	2.385	1.089, 1.090(2)		99.2(2), 102.2	116.9(3)	164.1		±59.7, 180.0
	$^4A''$	1.868	2.386	1.890, 1.090(2)		99.1, 100.6(2)	116.6, 117.0(2)	164.2		0.0, ±120.0
	$^4A_2$	1.889	2.484	1.087(3)		101.0(3)	116.5(3)	180.0		180.0(2)
TS2	$^2A'$	1.930, 1.950	1.967	1.093(2), 1.902	0.902	123.7(2)	105.8(2), 112.5	58.4, 85.3	26.9	±89.4(2)
	$^4A''$	1.888, 1.960	2.242	1.089(2), 1.227	1.310	60.7, 121.2(2)	113.1(2), 114.4	33.1, 72.8	39.8	±100.8
TS3	^2A	1.794, 1.811	2.036	1.091, 1.093, 2.047		52.7, 119.8, 127.0	105.0, 107.1, 112.6	64.0, 100.3		9.8, −86.5, 83.6, 179.9
	$^4A'$	1.837, 2.371	2.038	1.092(2), 1.937		55.0, 122.8(2)	103.1(2), 113.1	59.7, 138.7		±97.1, ±82.9
$(H)_2HfCH_2^+$	$^2A'$	1.787(2)	2.098	1.092(2)		123.8(2)	112.2	99.6(2)	102.6	±34.8, ±139.4
	$^4A_1$	1.937(2)	2.100	1.092(2)		123.9(2)	112.2	98.7(2)	162.6	±90.0(2)
	$^4A''$	1.790, 2.005	2.181	1.089, 1.090		116.6, 121.5	121.9	97.8, 160.1	102.1	0.0(2), 180.0(2)
	$^4A_1$	1.927(2)	2.113	1.092(2)		123.9(2)	112.2	102.0(2)	156.0	0.0(2) 180.0(2)
TS4	^2A	2.374, 2.375	1.892	1.082, 1.128	0.755	87.8, 159.7	112.5	93.5, 94.3	18.3	−80.4, 83.0, −98.8, 101.4
	$^4A'$	1.968(2)	2.112	1.092(2)		121.6, 126.6	111.8	106.0(2)	87.1	±45.8, ±134.2
$(H_2)HfCH_2^+$	$^2A'$	1.974, 1.999	1.958	1.093(2)	0.850	123.7(2)	112.5	64.1, 88.8	24.7	±89.9(2)
	^2A	2.021, 2.053	1.907	1.085, 1.157	0.818	77.6, 180.0	102.4	68.4, 91.5	23.2	−1.1, −2.1, 92.8, 93.8
	$^2A'$	2.457, 2.481	1.884	1.081, 1.138	0.755	83.5, 164.6	111.9	134.5, 152.1	17.6	0.0(2), 180.0(2)
	$^2A''$	2.598, 2.748	2.088	1.090, 1.093	0.752	122.2, 125.7	112.1	146.7, 162.6	15.9	0.0(2), 180.0(2)
	$^4A'$	2.173(2)	2.108	1.090, 1.093	0.781	122.4, 125.9	111.7	120.5(2)	20.7	±12.0, ±168.0
	$^4A''$	2.141(2)	2.108	1.091(2)	0.787	123.8(2)	112.4	104.1(2)	21.2	±79.5, ±101.3
	$^4A_2$	2.206(2)	2.139	1.093(2)	0.783	125.5(2)	109.1	169.8(2)	20.4	0.0(2), 180.0(2)
	$^2A_1$	2.609(2)	2.418	1.096(2)	0.751	125.0(2)	110.0	171.7(2)	16.6	0.0(2), 180.0(2)

[a] Bond lengths are in Å. Bond angles are in degrees. Degeneracies are listed in parentheses.

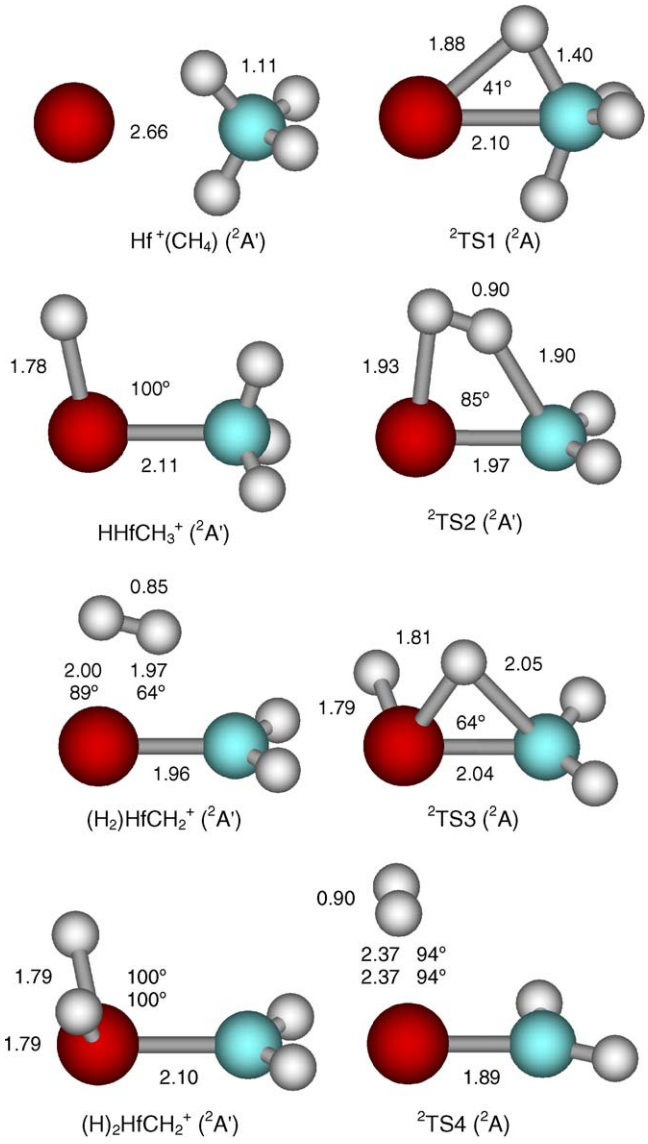

Fig. 5. Structures of several intermediates and transition states along the doublet surface of the [Hf,C,4H]+ system calculated at the B3LYP/HW+/6–311++G(3*df*,*sp*) level of theory. Bond lengths shown are in Ångstroms and HHfC bond angles are in degrees.

to Hf. From this intermediate, oxidative addition of a C–H bond to Hf^+ forms an $HHfCH_3^+$ insertion intermediate (Fig. 5), the global minimum on the PES. The transition state for oxidative addition, ^{2}TS1, has no symmetry and a H–Hf–C bond angle of 41°. The Hf–H bond distance, 1.88 Å, is longer than that of HfH^+ ($^3\Delta$), 1.79 Å, as is the Hf–C bond distance, 2.10 Å, compared to that of $HfCH_3^+$ ($^1A_1$), 2.07 Å. The energy of ^{2}TS1 lies above the energy of the reactants by 0.08 eV (Fig. 4), consistent with the fact that the 6*s* acceptor orbital on Hf^+ is doubly occupied in the ^{2}D state. The $HHfCH_3^+$ insertion intermediate has r(Hf–H) = 1.78 Å, r(Hf–C) = 2.11 Å, and ∠HHfC = 100° and a $^2A'$ ground state. These bond lengths are comparable to those of HfH^+ ($^3\Delta$) and $HfCH_3^+$ ($^1A_1$), indicating that covalent bonds to both H and CH_3 are formed. The singly occupied molecular orbital (SOMO) in this molecule is essentially a 6*s* nonbonding orbital on hafnium. A $^2A''$ excited state of this intermediate was also located. It has a similar geometry (Table 6), but now the SOMO is a nonbonding 5*d* (essentially the $5d_{xy}$) orbital on hafnium.

Continuing along the doublet surface, the $HHfCH_3^+$ intermediate can reductively eliminate H_2 to form a $(H_2)HfCH_2^+$ intermediate by proceeding through a four-centered transition state, ^{2}TS2. This $^2A'$ transition state has C_s symmetry and an Hf–C bond distance of 1.97 Å. The $(H_2)HfCH_2^+$ intermediate looks very similar to the transition state, retaining the $^2A'$ state and C_s symmetry. The Hf–C bond length is 1.96 Å, longer than the bond length in $HfCH_2^+$ ($^2A'$), 1.88 Å, indicating that the Hf–C double bond is not yet fully formed in this intermediate. Further, the H_2 bond distance is 0.85 Å as compared to that of free H_2, 0.74 Å, indicating that molecular hydrogen is electrostatically bound to the $HfCH_2^+$ molecule. Other states of $(H_2)HfCH_2^+$ were also located, each of which retains a relatively short H–H bond distance. For the lowest lying excited state, ^2A, the main distinction is that the CH_2 fragment has broken C_s symmetry by a rocking motion (see HfCH bond angles, Table 6). Whereas the $^2A'$ ground state has the center of the H_2 located perpendicular to the plane of the $HfCH_2$ molecule, the $^2A'$ state with an excitation energy of 0.29 eV has the H_2 center in this plane, as does the $^2A''$ state, which is heavily spin-contaminated (Table 5). There is also a $^2A_1$ state having C_{2v} symmetry where the H_2 center lies along the Hf–C bond axis, but this lies well above the ground state (3.74 eV).

Decomposition of $(H_2)HfCH_2^+$ by loss of H_2 results in the final dehydrogenation product, $HfCH_2^+$. Importantly, although $(H_2)HfCH_2^+$ ($^2A'$) is a stable intermediate on the PES, once zero point energy corrections are included, the energy of ^{2}TS2 lies below that of the intermediate by 0.02 eV (Table 5). Thus, reductive elimination of H_2 from $HHfCH_3^+$ is essentially a barrierless process to form products (Fig. 4).

An alternative mechanism for dehydrogenation of the $HHfCH_3^+$ intermediate involves sequential H atom transfers to form a $(H)_2HfCH_2^+$ ($^2A'$) dihydride intermediate (Fig. 5). This dihydride intermediate is relatively unstable because Hf^+ cannot simultaneously form four covalent bonds. Consequently, although the two Hf–H bond lengths, 1.79 Å each, are comparable to that of HfH^+ ($^3\Delta$), 1.79 Å, the Hf–C bond length of 2.10 Å is characteristic of a single covalent bond, such as in $HfCH_3^+$ ($^1A_1$), 2.07 Å, rather than that of the double bond in $HfCH_2^+$ ($^2A'$), 1.88 Å. The dihydride intermediate is reached via ^{2}TS3, which lies 0.17 eV below the reactants energy. Reductive elimination of H_2 from the dihydride intermediate carries the molecule across ^{2}TS4, which lies 0.08 eV above the reactants. The imaginary frequency (553 cm^{-1}) in ^{2}TS4 is essentially a rotation of the H_2 molecule that moves the hydrogens so that they are parallel with the HfC bond, as in $(H_2)HfCH_2^+$ ($^2A'$). Note that a lower energy pathway for transformation of $(H)_2HfCH_2^+$ ($^2A'$) to $(H_2)HfCH_2^+$ ($^2A'$) is actually to return to $HHfCH_3^+$ ($^2A'$) via ^{2}TS3 followed by ^{2}TS2 (Fig. 4). Overall, this alternate pathway for loss of H_2 from the $HHfCH_3^+$ intermediate is less favorable energetically by 0.27 eV compared to the four-centered pathway of ^{2}TS2.

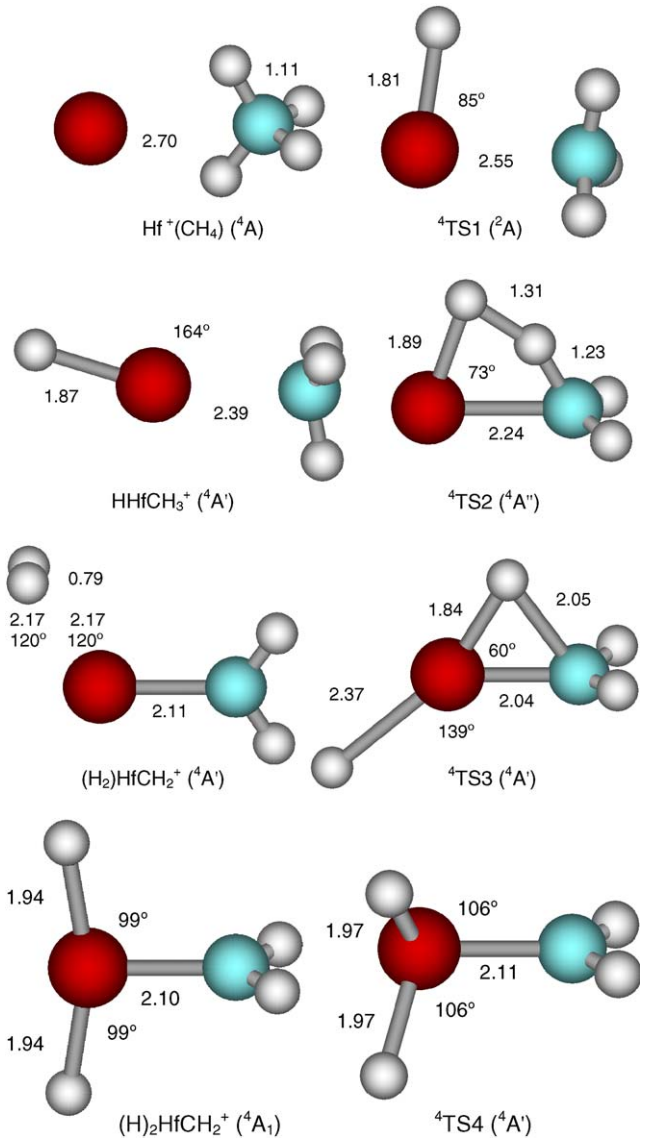

Fig. 6. Structures of several intermediates and transition states along the quartet surface of the [Hf,C,4H]+ system calculated at the B3LYP/HW+/6–311++G(3*df*,*sp*) level of theory. Bond lengths shown are in Ångstroms and HHfC bond angles are in degrees.

4.8. Quartet surface

On the quartet surface, the interaction of Hf^+ with methane leads to the formation of a $Hf^+(CH_4)$ adduct having no symmetry and a ^4A state (Fig. 6). This intermediate lies 0.27 eV above its analogue on the doublet surface, directly reflecting the calculated excitation energy of the Hf^+ (^4F) state. It has a valence configuration in the equivalent C_{2v} designation of $(1a_1)^1(1b_2)^1(2a_1)^1$ where the $1a_1$ is largely 6*s*, the $1b_2$ is $5d_{yz}$, and the $2a_1$ is $5d_{x2-y2}$, where the *xz*-plane is defined by the H atoms closest to Hf. We also located a $^4B_2$ state having C_{2v} symmetry, which lies 0.05 eV higher in energy and has a $(1a_1)^1(1b_2)^1(2a_1)^1$ configuration. It seems likely that these two states are actually degenerate. Oxidative addition of a C–H bond to Hf^+ leads to ^{4}TS1, which then forms the hydrido-methyl hafnium cation insertion intermediate, $HHfCH_3^+$ ($^4A'$) (Fig. 4). The transition state has no symmetry and a Hf–H bond length comparable to that of HfH^+ ($^3\Delta$), 1.79 Å, but a very long Hf–C bond, 2.55 Å, and an HHfC bond angle of 85°. The intermediate has C_s symmetry and a H–Hf–C bond angle of 164°. The Hf–H bond distance, 1.87 Å, is somewhat longer than that of HfH^+ ($^3\Delta$), 1.79 Å, but the Hf–C bond distance, 2.38 Å, is much larger than in $HfCH_3^+$ (^{1}A), 2.07 Å. This observation indicates that the methyl molecule is loosely bound to HfH^+ in this high spin state, consistent with the fact that two covalent bonds to Hf^+ cannot be formed given this high spin. Thus, both ^{4}TS1 and $HHfCH_3^+$ ($^4A'$) lie well above the analogous species on the doublet surface (Fig. 4). The $^4A''$ excited state of this intermediate differs from the $^4A'$ only in the dihedral angle (0° versus 180°) and lies only 0.01 eV higher in energy. The $^4A_2$ excited state lies much higher in energy (by 1.16 eV, Table 5). The geometry of this state has C_{3v} symmetry and an HHfC bond angle of 180° (Table 6).

As for the doublet surface, dehydrogenation of the $HHfCH_3^+$ ($^4A'$) intermediate occurs most readily over a four-centered transition state, ^{4}TS2 (Fig. 6). This $^4A''$ transition state has C_s symmetry and an Hf–C bond distance of 2.24 Å, much longer than the doublet analogue, again indicating the lack of a good covalent bond. This leads to the $(H_2)HfCH_2^+$ ($^4A'$) intermediate, which lies only 0.18 eV below the energy of the $HfCH_2^+$ ($^4B_2$)+H_2 product asymptote, consistent with a weakly bound H_2 molecule. Indeed, the H–H and Hf–C bond lengths in $(H_2)HfCH_2^+$ ($^4A'$) are 0.78 and 2.11 Å, respectively, comparable to free H_2 (0.74 Å) and $HfCH_2^+$ ($^4B_2$) (2.10 Å). Low-lying excited states of $(H_2)HfCH_2^+$ were also located. The $^4A''$ state (only 0.01 eV higher in energy) is similar to the $^4A'$ state except for the location of the H_2 molecule. In the $^4A'$ state, the center of the H_2 molecule lies in the plane defined by $HfCH_2$, whereas in the $^4A''$, it lies perpendicular to this plane. The $^4A_2$ excited state (0.54 eV higher in energy) has C_{2v} symmetry such that the center of the H_2 molecule lies on the same axis as the HfC bond.

Alternatively, the $HHfCH_3^+$ intermediate can transfer an α-H to form a dihydrido-methylidene hafnium cation intermediate $(H)_2HfCH_2^+$. The transition state for this motion, ^{4}TS3 ($^4A'$), has C_s symmetry and lies 2.60 eV above ground state reactants. The dihydride intermediate has C_{2v} symmetry ($^4A_1$ state) and lies high in energy, 2.13 eV above ground state reactants, because this high spin state cannot support the multiple bonds necessary. This is reflected in the Hf–C bond length of 2.10 Å, characteristic of a single covalent bond, and the Hf–H bond lengths of 1.94 Å, substantially longer than that of HfH^+ ($^3\Delta$), 1.79 Å. Excited states of the dihydride, $^4A''$ and $^4A_1$, lie only 0.16 and 0.50 eV, respectively, higher in energy (Table 5). The upper $^4A_1$ state has a similar geometry to the lower $^4A_1$ state but is planar, whereas the $^4A''$ state (also planar) has drastically changed one of the HHfC bond angles (Table 6). The dihydride converts to the $(H_2)HfCH_2^+$ intermediate through ^{4}TS4 ($^4A'$), lying 0.58 eV higher than the dihydride in energy. Clearly, this alternate pathway is again less favorable compared to the four-centered pathway involving ^{4}TS2, by 0.93 eV along the quartet surface.

5. Discussion

The dehydrogenation of methane by Hf^+ (^2D) (reaction (4)), is endothermic (Fig. 1). Reasonable agreement between theoretical and experimental BDEs indicates the $HfCH_2^+$ product is formed in its $^2A'$ ($^2A_1$) ground state at threshold. This process must occur without activation in energy in excess of the endothermicity of the reaction because Irikura and Beauchamp observed that the reverse of reaction (4) occurs at thermal energies [4]. Experimental evidence that this reaction occurs through a $HHfCH_3^+$ intermediate comes from the strong competition evident between the formation of $HfCH_2^+ + H_2$ and $HfH^+ + CH_3$.

5.1. σ-Bond activation

Even with a detailed PES in hand, it is useful to consider the qualitative aspects involved in understanding σ-bond activation by atomic metal ions. A simple donor–acceptor model predicts that σ-bond activation requires an electronic configuration on the metal in which there is an acceptor orbital into which the electrons of the bond to be broken can be donated. Concomitantly, metal electrons in orbitals with π-like symmetry backdonate into the antibonding orbital of the bond to be broken [7,10]. For hafnium, the 6*s* acceptor orbital is doubly occupied in the ^2D ground state and a repulsive interaction takes place at TS1 on the PES, leading to an inefficient reaction. This can explain the relatively low reactivity of the hafnium metal cation.

This qualitative picture can also be used to understand why the back reaction of $HfCH_2^+$ ($^2A'$, $^2A_1$) adds H_2 in a barrierless process to form $HHfCH_3^+$. The valence orbitals of the hafnium methylidene cation are $(1a'_b)^2(1a''_b)^2(2a')^1$, where the $1a'_b$ and $1a''_b$ orbitals are the σ(a_1) and π(b_1) Hf–C bonding orbitals, and the 2a′ is a $6s$–$5d_{z2}$ nonbonding hybrid orbital on Hf. The lowest-lying unoccupied molecular orbitals include 3a′ (a_1, $5d_{x2-y2}$), 2a″ (a_2, $5d_{xy}$), 4a′ (b_2, $5d_{xz}$), and $3a''^*$ (π^*, b_1^*). In this case, the acceptor orbital on $HfCH_2^+$ is probably the empty 3a′, whereas the donor orbital is the $1a''_b$. As H_2 adds to Hf^+ along the Hf–C bond, the π backdonation has the right symmetry to break the H_2 bond and lead to formation of Hf–H and C–H covalent bonds. The availability of the empty 3a′ orbital on Hf allows a close approach, although there is undoubtedly mixing with the other a′ orbitals as well.

5.2. Mechanism for higher energy products

Simple bond cleavages of the H–Hf^+–CH_3 intermediate at energies beginning near 2.5 eV lead to HfH^+ and $HfCH_3^+$ products. These processes deplete the population of this intermediate, leading to a corresponding decline in the cross section for the dehydrogenation process. Because the formation of $HfCH_2^+ + H_2$ is thermodynamically preferred by about 2.1 eV (Table 1), this competition indicates that formation of $HfH^+ + CH_3$ is kinetically preferred, consistent with a simple bond cleavage compared to the more complex dehydrogenation process.

In the reaction of Hf^+ with CH_4 (CD_4), the HfH^+ (HfD^+) cross section is dominant at energies above about 3 eV (Fig. 1). This is characteristic behavior for the reaction of bare metal ions with hydrogen-containing polyatomic molecules [9,45,47,48]. The fact that the $HfH^+ + CH_3$ ($HfD^+ + CD_3^+$) channel dominates the $HfCH_3^+ + H$ ($HfCD_3^+ + D$) channel is a result of angular momentum constraints [9,45,49,50]. Because the $HfCH_3^+ + H$ ($HfCD_3^+ + D$) channel has a reduced mass of 1.0 (2.0) amu as compared to the reactants 14.7 (18.0) amu, it is only formed by reactants that come together with small orbital angular momenta, i.e., at small impact parameters. In contrast, the $HfH^+ + CH_3$ ($HfD^+ + CD_3$) has a reduced mass of 13.9 (16.4) amu, much closer to that of the reactants, such that most impact parameters leading to strong interactions between the Hf^+ and methane can form these products and still conserve angular momentum.

6. Conclusion

Ground state Hf^+ (^2D) ions react with methane yielding products over a broad range of kinetic energies. At low energies, $HfCH_2^+$ dominates the product spectrum but is formed in an endothermic reaction pathway. At higher energies, HfH^+ is the predominant species. Although the $HfCH_3^+$ channel shares a common energy threshold with the HfH^+ species, the latter product is favored because of angular momentum constraints. Dehydrogenation of $HfCH_3^+$, resulting in the $HfCH^+$ product, reduces its cross section at higher energies.

Ab initio calculations verify that all transition states and intermediates have doublet ground states, guaranteeing that the dehydrogenation reaction pathway is spin allowed. The PES shows that Hf^+ reacts with methane by oxidative addition of a C–H bond resulting in a hydrido-methyl hafnium intermediate, $HHfCH_3^+$. This is shown to be the global minimum on the PES. At elevated energies, simple bond cleavage from this intermediate yields the $HfH^+ + CH_3$ and $HfCH_3^+ + H$ products. The activation of a second C–H bond occurs through a four-centered transition state, $^2TS2$, forming a $(H_2)HfCH_2^+$ intermediate, in which molecular hydrogen is electrostatically bound to the hafnium methylidene cation. Elimination of H_2 from this latter intermediate forms the metal methylidene ion product. Once zero point energies are included, it is found that the reductive elimination of H_2 from the $HHfCH_3^+$ intermediate occurs directly with no barriers in excess of the endothermicity.

The low relative reactivity of Hf^+ (^2D) compared with other third-row transition metal cations can be traced to its $6s^25d^1$ electronic configuration, as originally suggested by Irikura and Beauchamp [4] over a decade ago. The present study reveals that the doubly occupied 6*s* orbital results in a relatively high barrier for the oxidative addition of a CH bond to Hf^+ (^2D) and to a relatively weak Hf^+–CH_2 bond. Indeed, Hf^+–CH_x BDEs are actually slightly weaker than those of the second-row congener, Zr^+–CH_x, and only slightly stronger than those of the first-row congener, Ti^+–CH_x. In addition, our calculations indicate that coupling to a ^4F state having a $6s^15d^2$ electronic configuration is not efficient as the high spin of this state results in a potential energy surface for reaction with methane that remains well above

the ground state doublet PES throughout the course of the reaction. Nevertheless, we find that the reactivity of methane with Hf^+ (^2D, $6s^25d^1$) is still greater than that of Lu^+ (^1S, $6s^2$) [9], which is probably related to the relative abilities to mix in some $6s^15d^{n+1}$ character. For Hf^+, the ^4F ($6s^15d^2$) and ^2F ($6s^15d^2$) states lie only 0.563 and 1.483 eV, respectively, above the ^2D ground state, whereas for Lu^+, the ^3D ($6s^15d^1$) and ^1D ($6s^15d^1$) states lie 1.628 and 2.149 eV, respectively, above the ^1S ground state [11], making such mixing much more difficult.

Acknowledgement

This work is supported by the National Science Foundation, Grant No. CHE-0451477.

References

[1] J. Haggin, Chem. Eng. News 71 (1993) 27.
[2] B.K. Warren, S.T. Oyama, Heterogeneous Hydrocarbon Oxidation, ACS, Washington, DC, 1996.
[3] K.K. Irikura, J.L. Beauchamp, J. Am. Chem. Soc. 113 (1991) 2769.
[4] K.K. Irikura, J.L. Beauchamp, J. Phys. Chem. 95 (1991) 8344.
[5] Y.A. Ranasinghe, T.J. MacMahon, B.S. Freiser, J. Phys. Chem. 94 (1991) 7721.
[6] P.B. Armentrout, M.R. Sievers, J. Phys. Chem. A 107 (2003) 4396.
[7] P.B. Armentrout, J.L. Beauchamp, Acc. Chem. Res. 22 (1989) 315.
[8] L.S. Sunderlin, P.B. Armentrout, J. Phys. Chem. 92 (1988) 1209.
[9] L.S. Sunderlin, P.B. Armentrout, J. Am. Chem. Soc. 111 (1989) 3845.
[10] P.B. Armentrout, Organometallic Bonding and Reactivity, in: J.M. Brown, P. Hofmann (Eds.), Topics in Organometallic Chemistry, 4, Springer-Verlag, Berlin, 1999, p. 1.
[11] C.E. Moore, Atomic Energy Levels, III, NSRDS-NBS, 35, 1971, p. 1.
[12] S.K. Loh, D.A. Hales, L. Lian, P.B. Armentrout, J. Chem. Phys. 90 (1989) 5466.
[13] R.H. Schultz, P.B. Armentrout, Int. J. Mass Spectrom. Ion Processes 107 (1991) 29.
[14] E. Teloy, D. Gerlich, Chem. Phys. 4 (1974) 417.
[15] D. Gerlich, Adv. Chem. Phys. 82 (1992) 1.
[16] K.M. Ervin, P.B. Armentrout, J. Chem. Phys. 83 (1985) 166.
[17] P.J. Chantry, J. Chem. Phys. 55 (1971) 2746.
[18] C.L. Haynes, P.B. Armentrout, Organometallics 13 (1994) 3480.
[19] M.R. Sievers, Y.-M. Chen, J.L. Elkind, P.B. Armentrout, J. Phys. Chem. 100 (1996) 54.
[20] B.L. Kickel, P.B. Armentrout, J. Am. Chem. Soc. 117 (1995) 4057.
[21] B.L. Kickel, P.B. Armentrout, J. Am. Chem. Soc. 117 (1995) 764.
[22] D.E. Clemmer, Y.-M. Chen, F.A. Khan, P.B. Armentrout, J. Phys. Chem. 98 (1994) 6522.
[23] W.J. Chesnavich, M.T. Bowers, J. Phys. Chem. 83 (1979) 900.
[24] N. Aristov, P.B. Armentrout, J. Am. Chem. Soc. 108 (1986) 1806.
[25] P.B. Armentrout, in: N.G. Adams, L.M. Babcock (Eds.), Advances in Gas-Phase Ion Chemistry, I, JAI, Greenwhich, CT, 1992, p. 83.
[26] T. Shimanouchi, Tables of Molecular Vibrational Frequencies, consolidated I, NSRDS-NBS39, Washington, DC, 1972, p. 1.
[27] M.T. Rodgers, P.B. Armentrout, J. Chem. Phys. 109 (1998) 1787.
[28] A.D. Becke, J. Chem. Phys. 98 (1993) 5648.
[29] C. Lee, W. Yang, R.G. Parr, Phys. Rev. B 37 (1988) 785.
[30] M.J. Frisch, G.W. Trucks, H.B. Schlegel, G.E. Scuseria, M.A. Robb, J.R. Cheeseman, J.A. Montgomery, T. Vreven, K.N. Kudin, J.C. Burant, J.M. Millam, S.S. Iyengar, J. Tomasi, V. Barone, B. Mennucci, M. Cossi, G. Scalmani, N. Rega, G.A. Petersson, H. Nakatsuji, M. Hada, M. Ehara, K. Toyota, R. Fukuda, J. Hasegawa, M. Ishida, T. Nakajima, Y. Honda, O. Kitao, H. Nakai, M. Klene, X. Li, J.E. Knox, H.P. Hratchian, J.B. Cross, C. Adamo, J. Jaramillo, R. Gomperts, R.E. Stratmann, O. Yazyev, A.J. Austin, R. Cammi, C. Pomelli, J.W. Ochterski, P.Y. Ayala, K. Morokuma, G.A. Voth, P. Salvador, J.J. Dannenberg, V.G. Zakrzewski, S. Dapprich, A.D. Daniels, M.C. Strain, O. Farkas, D.K. Malick, A.D. Rabuck, K. Raghavachari, J.B. Foresman, J.V. Ortiz, Q. Cui, A.G. Baboul, S. Clifford, J. Cioslowski, B.B. Stefanov, G. Liu, A. Liashenko, P. Piskorz, I. Komaromi, R.L. Martin, D.J. Fox, T. Keith, M.A. Al-Laham, C.Y. Peng, A. Nanayakkara, M. Challacombe, P.M.W. Gill, B. Johnson, W. Chen, M.W. Wong, C. Gonzalez, J.A. Pople, Gaussian 03, Revision B. 02, Gaussian, Inc., Pittsburgh, PA, 2003.
[31] X.-G. Zhang, R. Liyanage, P.B. Armentrout, J. Am. Chem. Soc. 123 (2001) 5563.
[32] M.M. Armentrout, F.-X. Li, P.B. Armentrout, J. Am. Chem. Soc. 108 (2004) 9660.
[33] P.B. Armentrout, S. Shin, R. Liyanage, J. Phys. Chem. A. 110 (2006) 1242.
[34] F.-X. Li, X.-G. Zhang, P.B. Armentrout, Int. J. Mass Spectrom., accepted for publication.
[35] P.J. Hay, W.R. Wadt, J. Chem. Phys. 82 (1985) 299.
[36] G. Ohanessian, M.J. Brusich, W.A. Goddard III, J. Am. Chem. Soc. 112 (1990) 7182.
[37] M.C. Holthausen, C. Heinemann, H.H. Cornehl, W. Koch, H. Schwarz, J. Chem. Phys. 102 (1995) 4931.
[38] M.C. Holthausen, M. Mohr, W. Koch, Chem. Phys. Lett. 240 (1995) 245.
[39] D. Andrae, U. Haeussermann, M. Dolg, H. Stoll, H. Preuss, Theor. Chim. Acta 77 (1990) 123.
[40] C. Peng, H.B. Schlegel, Isr. J. Chem. 33 (1994) 449.
[41] C. Peng, P.Y. Ayala, H.B. Schlegel, M.J. Frisch, J. Comput. Chem. 17 (1996) 49.
[42] C. Hinton, P.B. Armentrout, work in progress.
[43] J. Simons, J. Nichols, Quantum Mechanics in Chemistry, Oxford University Press, New York, NY, 1997, p. 219.
[44] K.K. Irikura, W.A. Goddard III, J. Am. Chem. Soc. 116 (1994) 8733.
[45] P.B. Armentrout, B.L. Kickel, in: B.S. Freiser (Ed.), Organometallic Ion Chemistry, Kluwer, Dordrecht, The Netherlands, 1996, p. 1.
[46] M.R. Sievers, P.B. Armentrout, Organometallics 22 (2003) 2599.
[47] N. Aristov, P.B. Armentrout, J. Phys. Chem. 91 (1987) 6178.
[48] Y.-M. Chen, M.R. Sievers, P.B. Armentrout, Int. J. Mass Spectrom. Ion Processes 167/168 (1997) 195.
[49] L.S. Sunderlin, P.B. Armentrout, J. Phys. Chem. 92 (1988) 1209.
[50] Y.-M. Chen, P.B. Armentrout, J. Phys. Chem. 99 (1995) 10775.